

pubs.acs.org/JPCL Letter

First Synthesis of Mn-Doped Cesium Lead Bromide Perovskite Magic Sized Clusters at Room Temperature

Ke Xu, Evan T. Vickers, Binbin Luo, A'Lester C. Allen, Eefei Chen, Graham Roseman, Qihui Wang, David S. Kliger, Glenn L. Millhauser, Wenjing Yang, Xueming Li,* and Jin Zhong Zhang*



Cite This: J. Phys. Chem. Lett. 2020, 11, 1162-1169



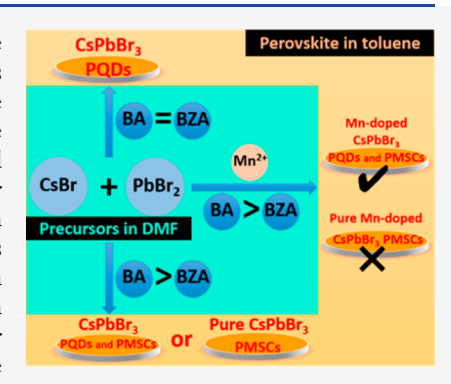
ACCESS

Metrics & More

Article Recommendations

s Supporting Information

ABSTRACT: Mn-doped CsPbBr₃ perovskite magic sized clusters (PMSCs) are synthesized for the first time using benzoic acid and benzylamine as passivating ligands and MnCl₂·4H₂O and MnBr₂ as the Mn²⁺ dopant sources at room temperature. The same approach is used to prepare Mn-doped CsPbBr₃ perovskite quantum dots (PQDs). The concentration of MnX₂ (X = Cl or Br) affects the excitonic absorption of the PMSCs and PQDs. A higher concentration of MnX₂ favors PMSCs over PQDs as well as higher photoluminescence (PL) quantum yields (QYs) and PL stability. The large ratio between the characteristic Mn emission (\sim 590 nm) and the host band-edge emission shows efficient energy transfer from the host exciton to the Mn²⁺ dopant. PL excitation, electron paramagnetic resonance, and time-resolved PL results all support Mn²⁺ doping in CsPbBr₃, which likely replaces Pb²⁺ ions. This study establishes a new method for synthesizing Mn-doped PMSCs with good PL stability, high PLQY and highly effective passivation.



C emiconductor magic sized clusters (MSCs) have attracted considerable attention due to their unique properties such as a narrow size distribution (often single sized) and utilization as building blocks for fabricating larger nanostructures with atomic precision.¹⁻³ MSCs are useful for studying the evolution of fundamental properties from molecules to quantum dots (QDs).4 Compared with conventional QDs, the MSCs usually can be associated with the occurrence of sharp peaks at persistent positions in optical absorption, which correspond to much narrower optical absorption bands.^{4–6} To date, II-VI semiconductor MSC materials, such as CdSe, CdS, ZnS, ZnTe, and CdTe, have been intensively studied in terms of chemical synthesis and theoretical investigations. 7-12 However, only a few studies have been reported on metal halide perovskite MSCs (PMSCs).^{3,6,13,14} The synthesis of lead halide PMSCs (APbX₃; $A = CH_3NH_3$ and Cs; X = Cl, Br, and I) has been reported. Recently, in our group, the growth and optical properties of methylammonium lead bromine (CH₃NH₃PbBr₃) and cesium lead bromide (CsPbBr₃) PMSCs were found to be strongly dependent on their capping ligand composition and concentration. 17,18

Doping is a key approach to altering the electronic, optical, and magnetic properties of bulk and nanostructured semi-conductors. For doped MSCs, examples includeMn-doped (CdSe)₁₃ MSCs, Cr-doped Si MSCs, Li-doped Al cluster anions, Mn-doped ZnTe magic sized nanocrystals, Pd-doped Au₃₈(SC₂H₄Ph)₂₄ MSCs, and Ti-doped Au MSCs.^{7,19–23} For lead halide perovskites (LHPs), doping has only been demonstrated for perovskite QDs (PQDs) using isovalent metal ions, such as alkaline-earth metal ions (Ba²⁺, Sr²⁺),

transition-metal ions (Mn²⁺, Zn²⁺, Cd²⁺, Ni²⁺), and heterovalent metal ions (Fe³⁺, Bi³⁺), which exhibit distinct optical and electronic properties compared with their undoped counterparts and have improved performance in device applications.²⁴⁻³⁰ However, to the best of our knowledge, there has been no report on doped PMSCs.

In this work, we demonstrate the first successful synthesis of Mn²⁺-doped CsPbBr₃ PMSCs using benzoic acid (BA) and benzylamine (BZA) as effective ligands together with manganese(II) chloride tetrahydrate (MnCl₂·4H₂O) or manganese(II) bromide (MnBr₂) as the Mn²⁺ source at room temperature. The same approach can be used to make Mn-doped CsPbBr₃ PQDs by adjusting the concentration of ligands. The amount of MnX_2 (X = Cl or Br) tunes the excitonic absorption of the PMSCs ($\lambda = 392-399$ nm) and PQDs ($\lambda = 454-471$ nm), with a higher concentration of MnX₂ favoring PMSCs over PQDs. All samples for Mn-doped CsPbBr₃ PMSCs and PQDs show a high photoluminescence (PL) quantum yield (QY) (ca. 55-84%) and PL stability, which are attributed to a low density of trap states due to effective passivation. On the basis of photoluminescence excitation (PLE), electron paramagnetic resonance (EPR), and time-resolved PL (TRPL) results, we suggest that Mn²⁺ is

Received: December 13, 2019 Accepted: January 22, 2020 Published: January 22, 2020



confirmed to be doped into the PMSCs and PQDs of CsPbBr₃. In addition, compared with MnBr₂, Mn²⁺ doping is more easily achieved with MnCl₂·4H₂O, as reflected by the stronger Mn emission, which possibly is attributed to the smaller ionic radius of Cl⁻ than Br⁻ and thereby the easier accommodation of the Mn²⁺ dopant.

Optical Properties and Exciton Dynamics of Undoped and Mn-Doped CsPbBr₃ PQDs and PMSCs. Figure 1a shows the

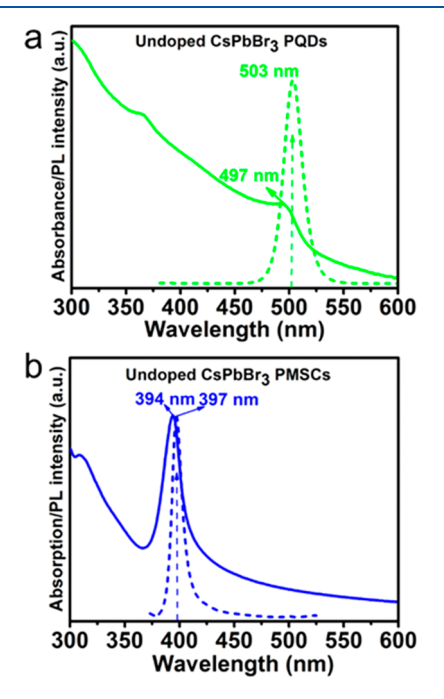


Figure 1. UV-vis absorption (solid) and PL (dashed) spectra for undoped (a) CsPbBr₃ PQDs and (b) CsPbBr₃ PMSCs samples.

ultraviolet-visible (UV-vis) absorption and PL spectra of the CsPbBr₃ PQDs sample, with absorption and emission peaks at 497 and 503 nm, respectively, and the PL with a full width at half-maximum (fwhm) of 20 nm. For the synthesis of CsPbBr₃ PQDs, relatively small amounts of BA and BZA as capping ligands were used, and the whole synthesis process was carried out at room temperature. When increasing the concentration of BA and BZA capping ligands, the UV-vis spectrum changed substantially, as shown in Figure 1b, with a strong absorption peak at 394 nm and an emission peak at 397 nm that has a fwhm of 11 nm. The significantly narrow PL bandwidth indicates the formation of CsPbBr₃ PMSCs. ¹⁵ With a relatively moderate concentration of passivating ligands, the synthesized product is a mixture of CsPbBr₃ PQDs and PMSCs. The corresponding UV-vis absorption and PL spectra of a CsPbBr₃ PQDs and PMSCs mixture are shown in Figure S1, which shows one strong and sharp excitonic absorption peak at 396 nm, a weaker and broader excitonic peak at 480 nm, and two emission peaks at 400 and 485 nm, with the bluer peaks for PMSCs and the redder peaks for PQDs, respectively. Therefore, more capping ligands favor CsPbBr₃ PMSCs over PQDs, as we previously found. 18 Whereas there are several reports about Mn-doped CsPbBr3 PQDs, there are no reports on Mn-doped CsPbBr₃ PMSCs.³¹ Our results on CsPbBr₃ PMSCs synthesized using MnCl₂·4H₂O and MnBr₂ as the Mn²⁺ source represent the first of their kind.

Figure 2a shows a photograph of Mn-doped CsPbBr₃ PMSCs and PQDs (with the amount of MnCl₂·4H₂O 0.10, 0.20, 0.30, and 0.40 mol) under the illumination of the UV lamp. With an increase in the MnCl₂·4H₂O concentration, the fluorescence color of the solution changed from green to blue, pink, and orange. As shown in Figure 2b, the UV—vis spectra of Mn-doped CsPbBr₃ PMSCs and PQDs with 0.10, 0.20, 0.30, and 0.40 mol MnCl₂·4H₂O have two or three excitonic

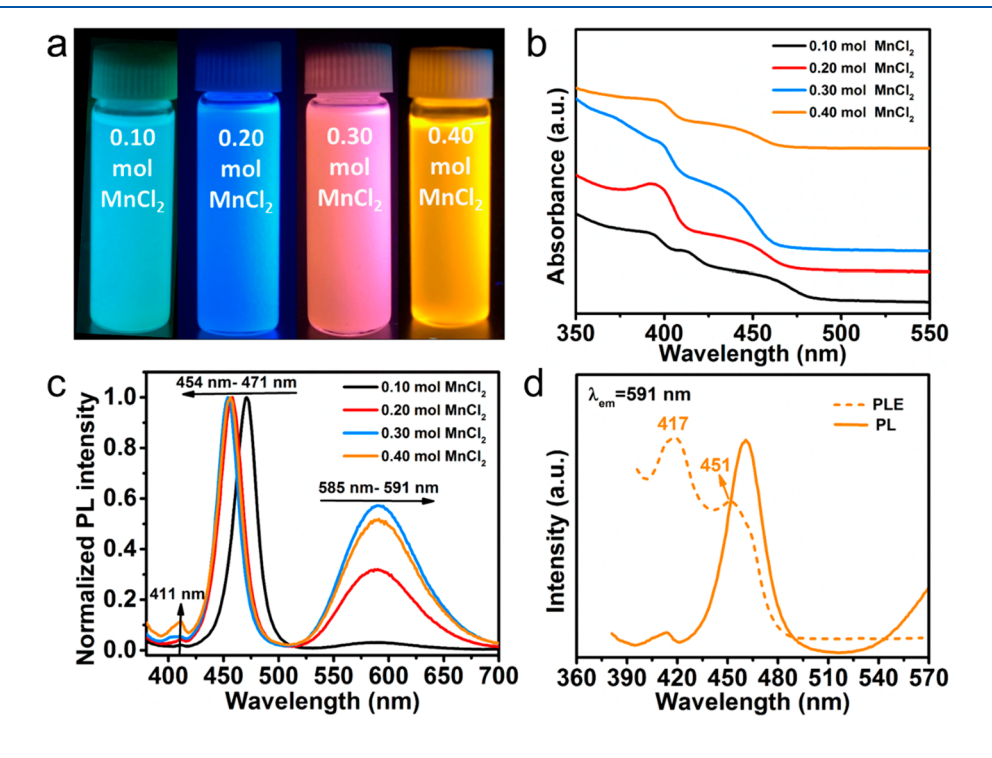


Figure 2. (a) Photograph of the samples in toluene under UV lamp irradiation (λ_{ex} = 365 nm). (b) UV—vis absorption and (c) PL spectra for Mndoped CsPbBr₃ PQDs and PMSCs samples with 0.10, 0.20, 0.30, and 0.40 mol MnCl₂·4H₂O. (d) PL and PLE spectra of Mn-doped CsPbBr₃ PQDs and PMSCs samples with 0.40 mol MnCl₂·4H₂O.

absorption peaks at 392/411/464, 395/452, 398/450, and 399/447 nm, respectively, whereas their PL spectra show emission peaks at 398/412/471/585, 411/455/589, 411/454/590, and 411/455/591 nm, respectively, as shown in Figure 2c. In particular, the broad emission band peak at $\sim\!590$ nm is characteristic of the Mn²+ emission band.³2-34 For the sample with 0.40 mol MnCl₂·4H₂O, the PLE spectrum measured with the emission wavelength at 591 nm shows two peaks at 417 and 451 nm, as shown in Figure 2d, which indicates that both the CsPbBr₃ PMSCs and CsPbBr₃ PQDs are doped with Mn²+.

Interestingly, with an increasing amount of MnCl₂·4H₂O, the PL emission peak for CsPbBr₃ PQDs shows a blue shift from 471 to 454 nm, whereas the PL emission peak attributed to CsPbBr₃ PMSCs (411 nm) remains unchanged. In addition, with the amount of MnCl₂·4H₂O increasing from 0.1 to 0.2 mol, the first excitonic UV-vis and PL peaks for PQDs blue shift from 464 to 452 nm and 471 to 455 nm, respectively. However, when the amount of MnCl₂·4H₂O is increased from 0.2 to 0.3 and 0.4 mol, the blue shifts for PQDs are both smaller. The blue shift for the PQDs is possibly due to the fact that the enhanced passivation by the additional Cl⁻ ions helps to better passivate Pb2+ and Cs+ surface defects, which result in smaller sized PQDs and thereby bluer excitonic absorption and PL. Another possible reason is that there is anion exchange between Cl⁻ and Br⁻ to increase the host band gap, producing a mixture of CsPb(Br/Cl)₃ and CsPbBr₃ PQDs. 55,36 With increasing MnCl₂·4H₂O concentration, the Mn²⁺ emission slightly shifts from 585 to 591 nm, indicating that the coordination environment of Mn2+ may have changed. The overall PLQYs for undoped and Mn-doped samples with various concentrations of MnCl₂·4H₂O (0.10, 0.20, 0.30, and 0.40 mol) were measured to be 42, 55, 67, 74, and 84%, respectively. The doped samples have higher PLQYs than the undoped sample, and the PLQY increases with increasing amount of MnCl₂·4H₂O, which is possibly due to the passivation effect of the Cl from MnCl₂·4H₂O and is consistent with previous reports.³⁷

In addition, we used isopropanol as a protonic solvent and air to evaluate the stability of undoped and Mn-doped samples, as shown in Figure S2a,b, respectively. Interestingly, the Mn-doped CsPbBr₃ PMSCs and PQDs are comparatively more stable than the undoped sample, possible due to the better passivation by the Cl⁻ ions introduced with the Mn²⁺ dopant.

As shown in Figure 3a, for undoped CsPbBr₃ PMSCs and PQDs in chloroform, the UV—vis absorption spectrum exhibits a strong and sharp excitonic absorption peak at 400 nm, whereas the PL spectrum exhibits two emission peaks at 402 and 474 nm. For the Mn-doped (MnBr₂) CsPbBr₃ PQDs and PMSCs, the UV—vis spectrum shows a strong and sharp excitonic absorption peak at 396 nm, with the PL spectrum showing three weak emission peaks at 398, 437, and 602 nm, where the 602 nm PL peak is attributed to the characteristic feature of d—d Mn emission.^{21,38}

To determine Mn²⁺ doping, we conducted EPR studies of Mn-doped (0.40 mol MnCl₂·4H₂O) CsPbBr₃ PQDs and PMSCs, BA/BZA/MnCl₂·4H₂O, BA/MnCl₂·4H₂O, and BZA/MnCl₂·4H₂O samples. As shown in Figure 4a, the doped samples showed the characteristic Mn²⁺ peaks.³⁹ The Mn²⁺ EPR signal was weaker after the sample was washed, as expected, because the Mn²⁺ ions in the solution can contribute to the signal.³³ The EPR signal for the final washed sample should mainly be due to Mn²⁺ doped into the PMSCs or

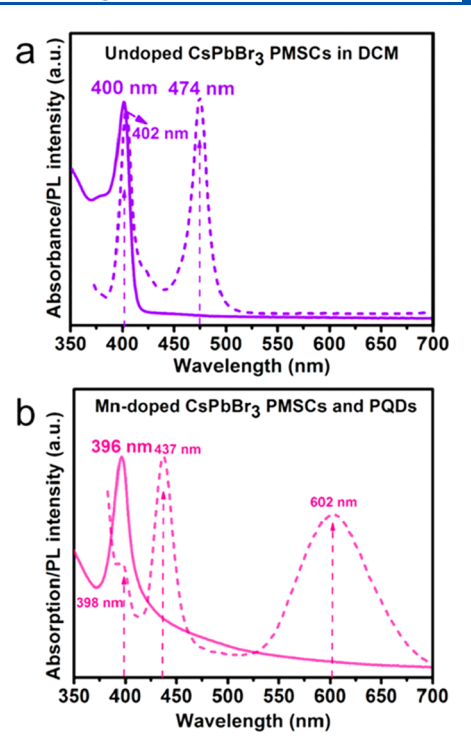


Figure 3. UV-vis absorption (solid line) and PL spectra (dashed line) showing (a) the undoped sample in chloroform and (b) the Mndoped (MnBr₂) sample in toluene, which exhibits a new emission peak (602 nm) corresponding to the Mn d-d transition.

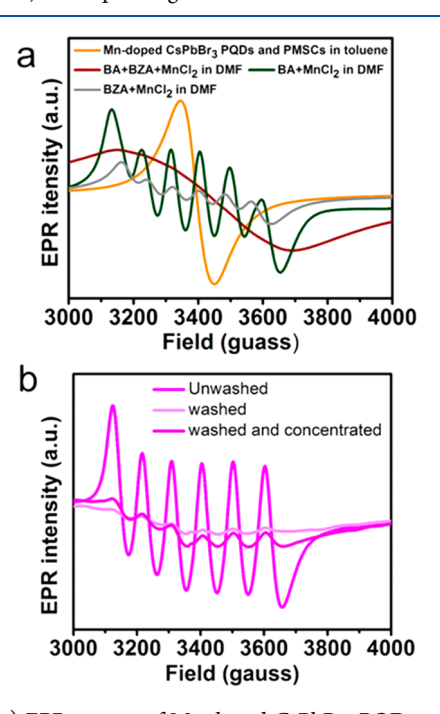


Figure 4. (a) EPR spectra of Mn-doped CsPbBr₃ PQDs and PMSCs, BA/BZA/MnCl₂·4H₂O, BA/MnCl₂·4H₂O, and BZA/MnCl₂·4H₂O samples. (b) EPR spectra of Mn-doped (MnBr₂) sample in toluene at room temperature.

PQDs. The broad features are likely due to the exchange interaction between neighboring Mn^{2+} ions.³³

Interestingly, when $MnBr_2$ was used as a source for Mn^{2+} for doping, all samples (unwashed, washed eight times, and washed and concentrated) showed the six hyperfine lines of Mn^{2+} . The results suggest that the salt for Mn^{2+} makes a

difference in the final doped products, possibly due to the role played by the counterion (Cl $^-$ vs Br $^-$ in this case). It is possible that Cl $^-$ can bridge two Mn $^{2+}$ ions while Br $^-$ cannot, resulting in the broad EPR spectrum for the sample with MnCl $_2\cdot 4H_2O$ as the Mn source. $^{40-42}$

To further establish $\rm Mn^{2+}$ doping, we usedTRPL to determine the PL lifetime. If $\rm Mn^{2+}$ doping was successful, then we would expect a PL with a lifetime on the order of the ~ 1.0 ms time scale, which is characteristic of a $\rm Mn^{2+}$ PL lifetime. $\rm ^{31,33,34}$ Figure 5 shows TRPL results obtained for

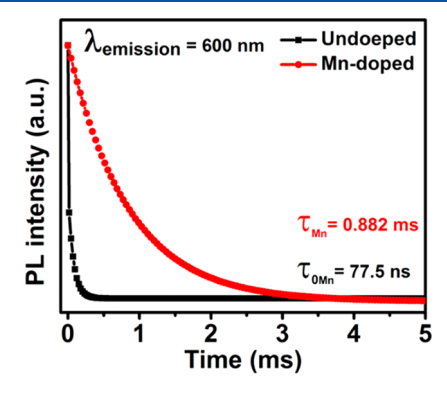


Figure 5. Normalized TRPL decay curves of the undoped and Mndoped CsPbBr₃ PQDs and PMSCs samples with 0.20 mol MnCl₂·4H₂O.

undoped and Mn-doped (0.20 mol MnCl₂·4H₂O) CsPbBr₃ PMSCs and PQDs by exciting at 355 nm and monitoring at 600 nm. For the undoped sample, there is a very weak PL signal at 600 nm with a lifetime of 77.5 ns, which can be attributed to trap states of the host material. Importantly, the PL lifetime from fitting the TRPL data is 0.882 ms for the doped samples, which can be assigned to Mn²⁺ emission due to the spin-forbidden transition from $^4\mathrm{T}_1$ to $^6\mathrm{A}_1$. This result clearly supports the successful doping of Mn²⁺ into the PMSCs and PQDs.

Structural Properties. X-ray diffraction (XRD) patterns (detailed in Figure S3a) of both undoped and Mn-doped CsPbBr₃ PQDs and PMSCs show a cubic-phase CsPbBr₃ perovskite structure with a space group of Pm3m (JCPDS no. 18-0364). With increasing MnCl₂·4H₂O, the XRD peaks become broader, which indicates a smaller size and a better passivation. In addition, some weak peaks are also observed in the small-angle region, which suggests that the XRD results may represent more of the aggregated or assembled large structures upon drying rather than the original CsPbBr₃ PQDs or PMSCs in solution, similar to what we previously found for undoped PMSCs.¹⁸ Interestingly, as shown in Figure S3b, the magnified view of the XRD data shows a small systematic shift in the peak position at $2\theta \approx$ 21.5° and a shift in the peak toward higher 2θ values with more Mn²⁺ doping. This shift suggests Mn²⁺ incorporation in the lattice of CsPbBr₃, where Mn²⁺ replaces Pb²⁺. The ionic radius of Mn^{2+} is 0.97 Å, which is significantly smaller than that for Pb^{2+} (1.33 Å). 44,45 Therefore, this decrease in the average cation size with increasing Mn²⁺ results in the shift of the XRD peaks toward higher angles. In addition, energy-dispersive Xray spectroscopy (EDS) was carried out for the Mn-doped CsPbBr₃ PQDs and PMSCs with 0.10 mol MnCl₂·4H₂O. The EDS mapping in Figure S4b-f shows the Cs, Pb, Mn, Br, and Cl elements, respectively, and the analysis verified the

formation of a uniform distribution of 0.33% mass percentage Mn²⁺ in the Mn-doped CsPbBr₃ PQDs and PMSCs (Figure S4g). Moreover, the high-angle annular dark-field scanning transmission microscopy (HAADF–STEM) image of Mn-doped CsPbBr₃ PQDs and PMSCs reveals the same large size as that in Figure S4a, which is similar to what has been reported in previous work related to PMSCs.⁴ The same occurred for QDs that aggregated into larger structures during the TEM grid preparation. Therefore, the observed TEM structures are not the same original isolated PMSC or PQD structures in solution that were measured by optical spectroscopy.

Electronic Properties by X-ray Photoelectron Spectroscopy. To characterize the chemical composition and covalent bonding of undoped and Mn-doped CsPbBr₃ PMSCs and PQDs, X-ray photoelectron spectroscopy (XPS) survey spectra were measured. As shown in Figure 6a, for the undoped CsPbBr₃ PMSC and PQD samples, the main peaks of Cs 3d_{3/2}, Cs 3d_{5/2}, O 1s, Pb $4d_{3/2}$, Pb $4d_{5/2}$, N 1s, C 1s, Br 3s, Pb $4f_{5/2}$, Pb $4f_{7/2}$, and Br 3d are clearly observed, respectively. At the same time, for the Mn-doped CsPbBr₃ PMSC and PQD samples, in addition to these peaks, the signals of Mn 2p, Cl 2s, and Cl 2p are observed at 130.6, 102.3, and 68.7 eV, respectively, indicating the Mn²⁺ doping of the CsPbBr₃ PMSCs and PQDs. 48 As shown in Figure 6b-d, for the undoped CsPbBr₃ PMSCs and PQDs, the Cs 3d, Pb 4f, and Br 3d spectra show the two Cs 3d peaks at 737.5 and 723.6 eV, the two Pb 4f peaks at 142.7 and 137.7 eV, and the two Br 3d peaks at 68.7 and 67.7 eV, which correspond to Cs $3d_{3/2}$ and Cs $3d_{5/2}$, Pb $4f_{5/2}$ and Pb $4f_{7/2}$, and Br $3d_{3/2}$ and Br $3d_{5/2}$ electron energy levels, respectively. Meanwhile, for the Mn-doped CsPbBr3 PMSCs and PQDs, the Cs 3d, Pb 4f and Br 3d spectra show the two Cs $3d_{3/2}$ and Cs $3d_{5/2}$ peaks at 737.6 and 723.7 eV, the two Pb $4f_{5/2}$ and Pb $4f_{7/2}$ peaks at 143.2 and 138.3 eV, and the two Br $3d_{3/2}$ and Br $3d_{5/2}$ peaks at 68.8 and 67.9 eV, respectively. Clearly, Cs 3d, Pb 4f, and Br 3d peaks are all shifted to larger binding energies, in particular, the Pb 4f and Br 4d peaks, and there is a positive shift (ca. 0.1/0.1, 0.5/ 0.6, 0.1/0.2 eV) from undoped to Mn-doped CsPbBr₃ PMSCs and PQDs. This may be due to coordination bonding of Cl-Cs, Cl-Pb, and Mn-Br on the surface of CsPbBr₃, with Cs 3d, Pb 4f, and Br 3d becoming more stable. In addition, compared with the Cs 3d and Br 3d peaks, the Pb 4f peaks have a larger red shift for the doped sample than the undoped sample, indicating a more modified chemical environment and changes in the electron density with Mn²⁺ doping.⁵²

To better understand the chemical bonding environment for Mn-doped CsPbBr₃ PMSCs and PQDs, Cl and Mn were more closely examined. As shown in Figure 6e,f, the Cl 2p peak can be fit with two peaks $(2p_{1/2}, 2p_{3/2})$ with binding energies of 199.8 and 198.2 eV, whereas the Mn 3p peak can be fit with three peaks $(3p_{1/2}, 3p_{3/2})$ with binding energies of 653.5, 645.1, and 641.8 eV.^{48,53} The results reveal the presence of Mn and Cl in the Mn-doped CsPbBr₃ PMSCs and PQDs. Furthermore, compared with the standard XPS signal for Mn²⁺ at 642.0 eV, the binding energy peak at 645.1 eV, corresponding to Mn 2p core levels, is detected only in the Mn-doped CsPbBr₃ perovskite, indicating Mn²⁺ ions in the CsPbBr₃ structure.

Explanation of the Coproduction of Mn-Doped PQDs and PMSCs. On the basis of the analysis of all of the results, we summarize the key steps involved in the synthesis of Mn-doped and undoped CsPbBr₃ PMSCs and PQDs, as shown in Figure

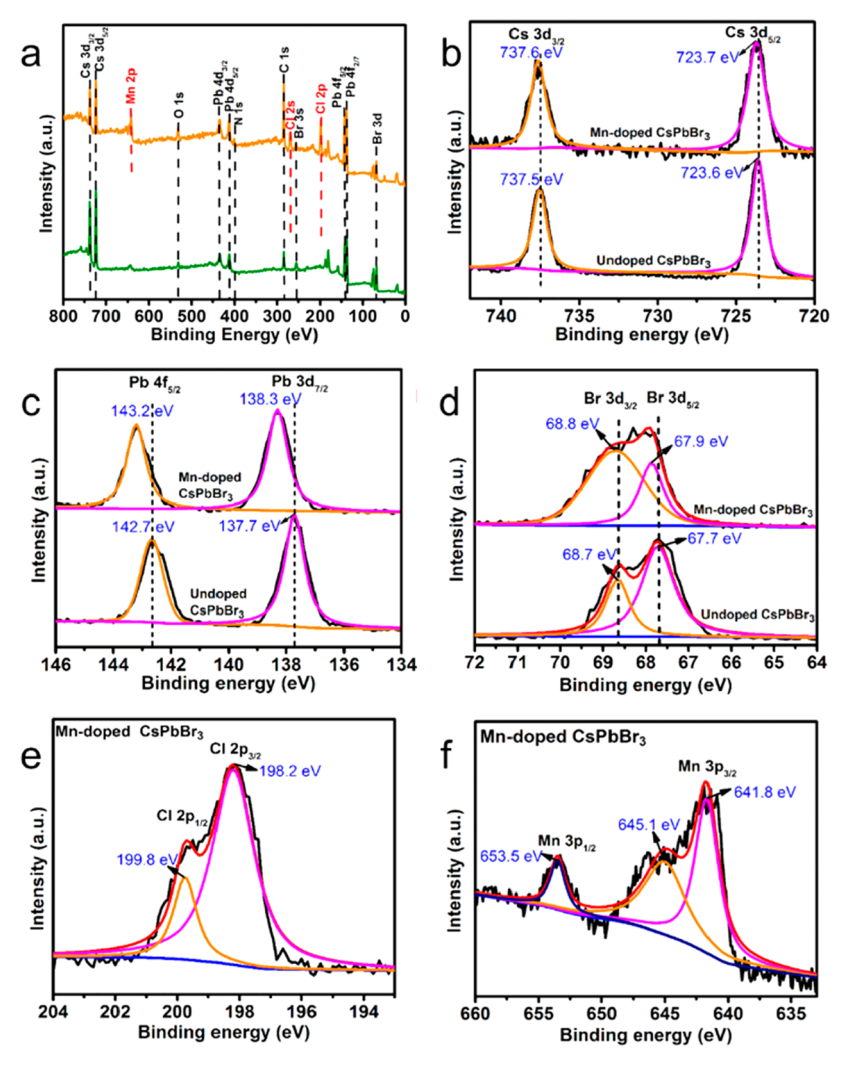


Figure 6. (a) XPS survey spectra of Mn-doped and undoped CsPbBr₃ PMSCs and PQDs. High-resolution XPS analysis of Mn-doped and undoped CsPbBr₃ PMSCs and PQDs corresponding to (b) Cs 3d, (c) Pb 4f, (d) Br 3d, (e) Cl 2p, and (f) Mn 3p.

7. For the synthesis of undoped samples, the product is CsPbBr₃ PQDs when the ratio of the BA and BZA as capping ligands is 1:1, whereas the product is a mixture of CsPbBr₃

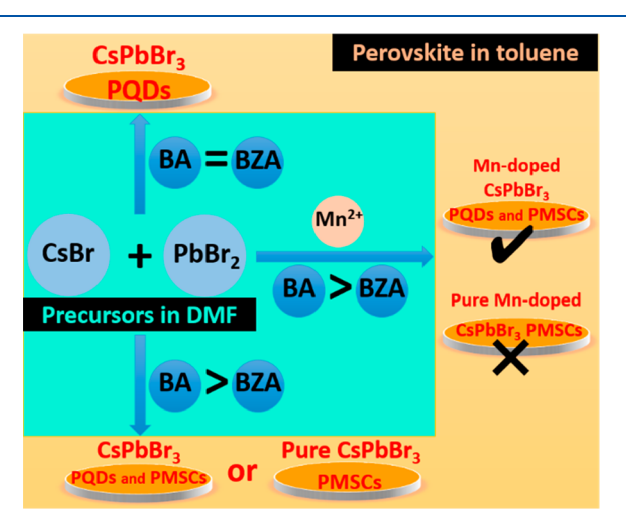


Figure 7. Schematic representation of Mn-doped and undoped CsPbBr₃ PMSCs and PQDs preparation.

PQDs and PMSCs or pure CsPbBr₃ PMSCs when the ratio of the BA and BZA is 1.05:1 or 1.2:1, respectively. Also, the concentration of BZA used for making pure CsPbBr₃ PODs is half that used for making pure CsPbBr₃ PMSCs or a mixture of CsPbBr₃ PQDs and PMSCs. Therefore, the ratio of CsPbBr₃ PQDs and CsPbBr3 PMSCs depends on the ratio and concentrations of BA and BZA, with more BA favoring CsPbBr₃ PMSCs. This is consistent with literature findings that an equal molar ratio of organic acid/base as capping ligands results in the formation of PQDs, whereas PMSCs start to be produced when the organic acid/base ratio is larger than one.¹⁷ However, for the synthesis of Mn-doped samples, only mixtures of CsPbBr3 PMSCs and PQDs can be produced, even with a BA/BZA ratio larger than one, and no pure Mndoped CsPbBr3 PMSCs could be produced at the BA/BZA ratio that produced pure undoped PMSCs.

Previous studies of Mn-doped PQDs found that their characteristic absorption and host emission peaks shift slightly (<20 nm) toward the blue compared with undoped PQDs. For pure Mn-doped II—VI semiconductors, doping does not alter the absorption and host emission positions. $^{5,34,54-57}$ In our case, when MnX₂ is added to the reaction under the same experimental conditions as those in the synthesis of pure CsPbBr₃ PMSCs, a mixture of Mn-doped CsPbBr₃ PMSCs and

PQDs was produced. It has not been possible so far to generate pure Mn-doped CsPbBr₃ PMSCs. This is possibly because the MnX₂ changes the original acid/base equilibrium in the solution so the ratio between CsPbBr₃ PQDs and CsPbBr₃ PMSCs generated is changed. It is also possible that MnX₂ facilitates the growth of CsPbBr₃ PMSCs into larger CsPbBr₃ PMSCs or CsPbBr₃ PQDs. Therefore, interestingly, the results show that the synthesis of pure Mn-doped CsPbBr₃ PMSCs is sensitive to the Mn precursors used. Further study is needed to clarify their exact role in determining the formation of PMSCs versus PQDs.

In summary, we report the first successful synthesis of Mndoped CsPbBr₃ PMSCs using BA and BZA as capping ligands together with MnCl₂·4H₂O or MnBr₂ as the Mn²⁺ source at room temperature, and Mn-doped CsPbBr3 PQDs also can be generated. The amount of Mn precursor used is found to affect the excitonic absorption ($\lambda = 392-399$ nm) of the PMSCs and PQDs ($\lambda = 454-471$ nm), with more MnX₂ favoring PMSCs over PQDs and resulting in a bluer absorption. This is possibly due to the counteranions used (Cl⁻ and Br⁻) that serve to passivate the PMSCs or PQDs. Both the Mn-doped CsPbBr₃ PMSCs and PQDs show high PLQY (ca. 55-84%) and good PL stability, reflecting effective passivation and a low density of band-gap trap states. The PLE, EPR, and TRPL results all support Mn²⁺ doping into the CsPbBr₃ PMSCs and PQDs. In particular, PLE as a direct experimental evidence proves the doping of Mn for CsPbBr₃ PMSCs and PQDs. In addition, compared with MnBr₂, the Mn²⁺ doping is more easily achieved with MnCl₂·4H₂O as the Mn source, as evidenced by stronger Mn emission, which is attributed to the smaller radius of Cl- compared with Br- and thereby a better accommodation of the Mn²⁺ ions. This work demonstrates the first synthesis of Mn-doped PMSCs that are promising for emerging optoelectronic applications such as single-photon emitters.

ASSOCIATED CONTENT

Supporting Information

The Supporting Information is available free of charge at https://pubs.acs.org/doi/10.1021/acs.jpclett.9b03700.

Details of experimental methods, UV-vis absorption and PL spectra of a mixture of CsPbBr₃ PQDs and PMSCs, stability study and XRD for undoped Mn-doped CsPbBr₃ PMSCs and PQDs, the HAADF-STEM image, elemental mappings, and energy-dispersive X-ray spectroscopy of Mn²⁺-doped CsPbBr₃ PQDs and PMSCs (PDF)

AUTHOR INFORMATION

Corresponding Authors

Xueming Li — College of Chemistry and Chemical Engineering, Chongqing University, Chongqing 400044, P. R. China; Email: xuemingli@cqu.edu.cn

Jin Zhong Zhang — Department of Chemistry and Biochemistry, University of California, Santa Cruz, California 95064, United States; orcid.org/0000-0003-3437-912X; Email: zhang@ucsc.edu

Authors

Ke Xu – Department of Chemistry and Biochemistry, University of California, Santa Cruz, California 95064, United States;

- College of Chemistry and Chemical Engineering, Chongqing University, Chongqing 400044, P. R. China
- Evan T. Vickers Department of Chemistry and Biochemistry, University of California, Santa Cruz, California 95064, United States; Occid.org/0000-0002-9594-4279
- Binbin Luo Department of Chemistry, Shantou University, Guangdong 515063, P. R. China; orcid.org/0000-0001-9652-7998
- A'Lester C. Allen Department of Chemistry and Biochemistry, University of California, Santa Cruz, California 95064, United States
- Eefei Chen Department of Chemistry and Biochemistry, University of California, Santa Cruz, California 95064, United States; ⊚ orcid.org/0000-0001-7411-7779
- **Graham Roseman** Department of Chemistry and Biochemistry, University of California, Santa Cruz, California 95064, United States
- Qihui Wang College of Chemistry and Chemical Engineering, Chongqing University, Chongqing 400044, P. R. China
- David S. Kliger Department of Chemistry and Biochemistry, University of California, Santa Cruz, California 95064, United States; Occid.org/0000-0003-4083-7369
- Glenn L. Millhauser Department of Chemistry and Biochemistry, University of California, Santa Cruz, California 95064, United States; orcid.org/0000-0003-2442-7220
- Wenjing Yang College of Chemistry and Chemical Engineering, Chongqing University, Chongqing 400044, P. R. China

Complete contact information is available at: https://pubs.acs.org/10.1021/acs.jpclett.9b03700

Notes

The authors declare no competing financial interest.

ACKNOWLEDGMENTS

This research was supported by NASA through MACES (NNX15AQ01A), the NSF (CHE 1904547), an NIH grant (R35GM131781), the Fundamental Research Funds for the Central Universities (no. 2018CDGFHG0012), JG2018103 (no. SKL-ACPS-C-03), and a UCSC Committee on Research Special Research Grant. K.X. is grateful for financial support from the program of the China Scholarship Council (CSC). B.L. acknowledges the support from the National Natural Science Foundation of China (NSFC: 51702205) and the STU Scientific Research Foundation for Talents (NTF17001). Work at the Molecular Foundry was supported by the Office of Science, Office of Basic Energy Sciences of the U.S. Department of Energy under contract no. DE-AC02-05CH11231.

REFERENCES

- (1) Kudera, S.; Zanella, M.; Giannini, C.; Rizzo, A.; Li, Y.; Gigli, G.; Cingolani, R.; Ciccarella, G.; Spahl, W.; Parak, W. J.; Manna, L. Sequential Growth of Magic-Size CdSe Nanocrystals. *Adv. Mater.* **2007**, *19* (4), 548–552.
- (2) Ningthoujam, R. S.; Gautam, A.; Padma, N. Oleylamine as a Reducing Agent in Syntheses of Magic-Size Clusters and Monodisperse Quantum Dots: Optical and Photoconductivity Studies. *Phys. Chem. Chem. Phys.* **2017**, *19* (3), 2294–2303.
- (3) Zhu, D.; Hui, J.; Rowell, N.; Liu, Y.; Chen, Q. Y.; Steegemans, T.; Fan, H.; Zhang, M.; Yu, K. Interpreting the Ultraviolet Absorption in the Spectrum of 415 nm-Bandgap CdSe Magic-Size Clusters. *J. Phys. Chem. Lett.* **2018**, 9 (11), 2818–2824.

- (4) Wang, L.; Hui, J.; Tang, J.; Rowell, N.; Zhang, B.; Zhu, T.; Zhang, M.; Hao, X.; Fan, H.; Zeng, J.; Han, S.; Yu, K. Precursor Self-Assembly Identified as a General Pathway for Colloidal Semiconductor Magic-Size Clusters. *Adv. Sci.* (Weinh) **2018**, 5 (12), 1800632.
- (5) Yang, J.; Muckel, F.; Baek, W.; Fainblat, R.; Chang, H.; Bacher, G.; Hyeon, T. Chemical Synthesis, Doping, and Transformation of Magic-Sized Semiconductor Alloy Nanoclusters. *J. Am. Chem. Soc.* **2017**, *139* (19), *6761–6770*.
- (6) Wang, Y.; Zhou, Y.; Zhang, Y.; Buhro, W. E. Magic-Size II-VI Nanoclusters as Synthons for Flat Colloidal Nanocrystals. *Inorg. Chem.* **2015**, *54* (3), 1165–77.
- (7) Eilers, J.; Groeneveld, E.; de Mello Donega, C.; Meijerink, A. Optical Properties of Mn-Doped ZnTe Magic Size Nanocrystals. J. Phys. Chem. Lett. 2012, 3 (12), 1663–7.
- (8) Azpiroz, J. M.; Matxain, J. M.; Infante, I.; Lopez, X.; Ugalde, J. M. A DFT/TDDFT Study on the Optoelectronic Properties of the Amine-Capped Magic (CdSe)₁₃ Nanocluster. *Phys. Chem. Chem. Phys.* **2013**, *15* (26), 10996–1005.
- (9) Botti, S.; Marques, M. A. L. Identification of Fullerene-Like CdSe Nanoparticles from Optical Spectroscopy Calculations. *Phys. Rev. B: Condens. Matter Mater. Phys.* **2007**, 75 (3), 035311.
- (10) Del Ben, M.; Havenith, R. W. A.; Broer, R.; Stener, M. Density Functional Study on the Morphology and Photoabsorption of CdSe Nanoclusters. *J. Phys. Chem. C* **2011**, *115* (34), 16782–16796.
- (11) Groeneveld, E.; van Berkum, S.; Meijerink, A.; de Mello Donega, C. Growth and Stability of ZnTe Magic-Size Nanocrystals. *Small* **2011**, 7 (9), 1247–56.
- (12) Wang, Y.; Liu, Y. H.; Zhang, Y.; Wang, F.; Kowalski, P. J.; Rohrs, H. W.; Loomis, R. A.; Gross, M. L.; Buhro, W. E. Isolation of the Magic-Size CdSe Nanoclusters [(CdSe)₁₃(n-octylamine)₁₃] and [(CdSe)₁₃(oleylamine)₁₃]. *Angew. Chem., Int. Ed.* **2012**, *51* (25), 6154–7.
- (13) Zhang, B.; Zhu, T.; Ou, M.; Rowell, N.; Fan, H.; Han, J.; Tan, L.; Dove, M. T.; Ren, Y.; Zuo, X.; Han, S.; Zeng, J.; Yu, K. Thermally-Induced Reversible Structural Isomerization in Colloidal Semi-conductor CdS Magic-Size Clusters. *Nat. Commun.* **2018**, *9* (1), 2499.
- (14) Voznyy, O.; Mokkath, J. H.; Jain, A.; Sargent, E. H.; Schwingenschlögl, U. Computational Study of Magic-Size CdSe Clusters with Complementary Passivation by Carboxylic and Amine Ligands. J. Phys. Chem. C 2016, 120 (18), 10015–10019.
- (15) Xu, Y.; Zhang, Q.; Lv, L.; Han, W.; Wu, G.; Yang, D.; Dong, A. Synthesis of Ultrasmall CsPbBr₃ Nanoclusters and Their Transformation to Highly Deep-Blue-Emitting Nanoribbons at Room Temperature. *Nanoscale* **2017**, *9* (44), 17248–17253.
- (16) Peng, L.; Geng, J.; Ai, L.; Zhang, Y.; Xie, R.; Yang, W. Room Temperature Synthesis of Ultra-Small, Near-Unity Single-Sized Lead Halide Perovskite Quantum Dots with Wide Color Emission Tunability, High Color Purity and High Brightness. *Nanotechnology* **2016**, *27* (33), 335604.
- (17) Vickers, E. T.; Xu, K.; Dreskin, B. W.; Graham, T. A.; Li, X.; Zhang, J. Z. Ligand Dependent Growth and Optical Properties of Hybrid Organo-metal Halide Perovskite Magic Sized Clusters. *J. Phys. Chem. C* 2019, 123 (30), 18746–18752.
- (18) Xu, K.; Allen, A. C.; Luo, B.; Vickers, E. T.; Wang, Q.; Hollingsworth, W. R.; Ayzner, A. L.; Li, X.; Zhang, J. Z. Tuning from Quantum Dots to Magic Sized Clusters of CsPbBr₃ Using Novel Planar Ligands Based on the Trivalent Nitrate Coordination Complex. J. Phys. Chem. Lett. 2019, 10 (15), 4409–4416.
- (19) Chen, M. X.; Yan, X. H. A New Magic Titanium-Doped Gold Cluster and Orientation Dependent Cluster-Cluster Interaction. *J. Chem. Phys.* **2008**, *128* (17), 174305.
- (20) Kawamura, H.; Kumar, V.; Kawazoe, Y. Growth, Magic Behavior, and Electronic and Vibrational Properties of Cr-Doped Si Clusters. *Phys. Rev. B: Condens. Matter Mater. Phys.* **2004**, 70 (24), 245433.
- (21) Muckel, F.; Yang, J.; Lorenz, S.; Baek, W.; Chang, H.; Hyeon, T.; Bacher, G.; Fainblat, R. Digital Doping in Magic-Sized CdSe Clusters. ACS Nano 2016, 10 (7), 7135–7141.

- (22) Negishi, Y.; Igarashi, K.; Munakata, K.; Ohgake, W.; Nobusada, K. Palladium Doping of Magic Gold Cluster Au₃₈(SC₂H₄Ph)₂₄: Formation of Pd₂Au₃₆(SC₂H₄Ph)₂₄ with Higher Stability than Au₃₈(SC₂H₄Ph)₂₄. Chem. Commun. (Cambridge, U. K.) **2012**, 48 (5), 660–662.
- (23) Zheng, W. J.; Thomas, O. C.; Lippa, T. P.; Xu, S. J.; Bowen, K. H., Jr. The ionic KAl₁₃ Molecule: A Stepping Stone to Cluster-Assembled Materials. *J. Chem. Phys.* **2006**, *124* (14), 144304.
- (24) Luo, B.; Li, F.; Xu, K.; Guo, Y.; Liu, Y.; Xia, Z.; Zhang, J. Z. B-Site Doped Lead Halide Perovskites: Synthesis, Band Engineering, Photophysics, and Light Emission Applications. *J. Mater. Chem. C* **2019**, 7 (10), 2781–2808.
- (25) Zhou, Y.; Chen, J.; Bakr, O. M.; Sun, H.-T. Metal-Doped Lead Halide Perovskites: Synthesis, Properties, and Optoelectronic Applications. *Chem. Mater.* **2018**, *30* (19), 6589–6613.
- (26) Das Adhikari, S.; Dutta, S. K.; Dutta, A.; Guria, A. K.; Pradhan, N. Chemically Tailoring the Dopant Emission in Manganese-Doped CsPbCl₃ Perovskite Nanocrystals. *Angew. Chem., Int. Ed.* **2017**, *56* (30), 8746–8750.
- (27) Liu, H.; Wu, Z.; Shao, J.; Yao, D.; Gao, H.; Liu, Y.; Yu, W.; Zhang, H.; Yang, B. CsPb_xMn_{1-x}Cl₃ Perovskite Quantum Dots with High Mn Substitution Ratio. *ACS Nano* **2017**, *11* (2), 2239–2247.
- (28) Arunkumar, P.; Gil, K. H.; Won, S.; Unithrattil, S.; Kim, Y. H.; Kim, H. J.; Im, W. B. Colloidal Organolead Halide Perovskite with a High Mn Solubility Limit: A Step Toward Pb-Free Luminescent Quantum Dots. J. Phys. Chem. Lett. 2017, 8 (17), 4161–4166.
- (29) Li, F.; Xia, Z.; Gong, Y.; Gu, L.; Liu, Q. Optical Properties of Mn²⁺ Doped Cesium Lead Halide Perovskite Nanocrystals via a Cation—Anion Co-Substitution Exchange Reaction. *J. Mater. Chem. C* **2017**, *5* (36), 9281—9287.
- (30) Zhou, G.; Jia, X.; Guo, S.; Molokeev, M.; Zhang, J.; Xia, Z. Role of Halogen Atoms on High-Efficiency Mn²⁺ Emission in Two-Dimensional Hybrid Perovskites. *J. Phys. Chem. Lett.* **2019**, *10* (16), 4706–4712.
- (31) Luo, B.; Guo, Y.; Li, X.; Xiao, Y.; Huang, X.; Zhang, J. Z. Efficient Trap-Mediated Mn²⁺ Dopant Emission in Two Dimensional Single-Layered Perovskite (CH₃CH₂NH₃)₂PbBr₄. *J. Phys. Chem. C* **2019**, 123 (23), 14239–14245.
- (32) Guner, T.; Akbali, B.; Ozcan, M.; Topcu, G.; Demir, M. M.; Sahin, H. Monitoring the Doping and Diffusion Characteristics of Mn Dopants in Cesium Lead Halide Perovskites. *J. Phys. Chem. C* **2018**, 122 (21), 11543–11549.
- (33) Mir, W. J.; Mahor, Y.; Lohar, A.; Jagadeeswararao, M.; Das, S.; Mahamuni, S.; Nag, A. Postsynthesis Doping of Mn and Yb into CsPbX₃ (X = Cl, Br, or I) Perovskite Nanocrystals for Downconversion Emission. *Chem. Mater.* **2018**, 30 (22), 8170–8178.
- (34) Parobek, D.; Dong, Y.; Qiao, T.; Son, D. H. Direct Hot-Injection Synthesis of Mn-Doped CsPbBr₃ Nanocrystals. *Chem. Mater.* **2018**, 30 (9), 2939–2944.
- (35) Guria, A. K.; Dutta, S. K.; Adhikari, S. D.; Pradhan, N. Doping Mn²⁺ in Lead Halide Perovskite Nanocrystals: Successes and Challenges. *ACS Energy Lett.* **2017**, *2* (5), 1014–1021.
- (36) Huang, G.; Wang, C.; Xu, S.; Zong, S.; Lu, J.; Wang, Z.; Lu, C.; Cui, Y. Postsynthetic Doping of MnCl₂ Molecules into Preformed CsPbBr₃ Perovskite Nanocrystals via a Halide Exchange-Driven Cation Exchange. *Adv. Mater.* **2017**, *29* (29), 1700095.
- (37) Zhou, S.; Zhu, Y.; Zhong, J.; Tian, F.; Huang, H.; Chen, J.; Chen, D. Chlorine-Additive-Promoted Incorporation of Mn²⁺ Dopants into CsPbCl₃ Perovskite Nanocrystals. *Nanoscale* **2019**, *11* (26), 12465–12470.
- (38) Pradhan, N. Red-Tuned Mn d-d Emission in Doped Semiconductor Nanocrystals. *ChemPhysChem* **2016**, *17* (8), 1087–94.
- (39) Pathak, N.; Gupta, S. K.; Ghosh, P. S.; Arya, A.; Natarajan, V.; Kadam, R. M. Probing Local Site Environments and Distribution of Manganese in SrZrO₃:Mn; PL and EPR Spectroscopy Complimented by DFT Calculations. *RSC Adv.* **2015**, *S* (23), 17501–17513.
- (40) Chen, D.; Zhou, S.; Fang, G.; Chen, X.; Zhong, J. Fast Room-Temperature Cation Exchange Synthesis of Mn-Doped CsPbCl₃

- Nanocrystals Driven by Dynamic Halogen Exchange. ACS Appl. Mater. Interfaces 2018, 10 (46), 39872-39878.
- (41) Liu, W.; Lin, Q.; Li, H.; Wu, K.; Robel, I.; Pietryga, J. M.; Klimov, V. I. Mn²⁺-Doped Lead Halide Perovskite Nanocrystals with Dual-Color Emission Controlled by Halide Content. *J. Am. Chem. Soc.* **2016**, *138* (45), 14954–14961.
- (42) Akkerman, Q. A.; Meggiolaro, D.; Dang, Z.; De Angelis, F.; Manna, L. Fluorescent Alloy $CsPb_xMn_{1-x}I_3$ Perovskite Nanocrystals with High Structural and Optical Stability. ACS Energy Lett. **2017**, 2 (9), 2183–2186.
- (43) Stoumpos, C. C.; Malliakas, C. D.; Peters, J. A.; Liu, Z.; Sebastian, M.; Im, J.; Chasapis, T. C.; Wibowo, A. C.; Chung, D. Y.; Freeman, A. J.; Wessels, B. W.; Kanatzidis, M. G. Crystal Growth of the Perovskite Semiconductor CsPbBr₃: A New Material for High-Energy Radiation Detection. *Cryst. Growth Des.* **2013**, *13* (7), 2722–2727
- (44) Mir, W. J.; Jagadeeswararao, M.; Das, S.; Nag, A. Colloidal Mn-Doped Cesium Lead Halide Perovskite Nanoplatelets. *ACS Energy Lett.* **2017**, 2 (3), 537–543.
- (45) Shannon, R. D. Revised Effective Ionic Radii and Systematic Studies of Interatomic Distances in Halides and Chalcogenides. *Acta Crystallogr., Sect. A: Cryst. Phys., Diffr., Theor. Gen. Crystallogr.* 1976, 32 (5), 751–767.
- (46) He, M.; Cheng, Y.; Yuan, R.; Zhou, L.; Jiang, J.; Xu, T.; Chen, W.; Liu, Z.; Xiang, W.; Liang, X. Mn-Doped Cesium Lead Halide Perovskite Nanocrystals with Dual-Color Emission for WLED. *Dyes Pigm.* **2018**, *152*, 146–154.
- (47) Xu, K.; Vickers, E. T.; Rao, L.; Lindley, S. A.; Allen, A. L. C.; Luo, B.; Li, X.; Zhang, J. Z. Synergistic Surface Passivation of CH₃NH₃PbBr₃ Perovskite Quantum Dots with Phosphonic Acid and (3-Aminopropyl) triethoxysilane. *Chem. Eur. J.* **2019**, 25 (19), 5014–5021.
- (48) He, M.; Cheng, Y.; Shen, L.; Zhang, H.; Shen, C.; Xiang, W.; Liang, X. Doping Manganese into CsPb(Cl/Br)₃ quantum Dots Glasses: Dual-Color Emission and Super Thermal Stability. *J. Am. Ceram. Soc.* **2019**, *102* (3), 1090–1100.
- (49) Chang, Y.; Yoon, Y. J.; Li, G.; Xu, E.; Yu, S.; Lu, C. H.; Wang, Z.; He, Y.; Lin, C. H.; Wagner, B. K.; Tsukruk, V. V.; Kang, Z.; Thadhani, N.; Jiang, Y.; Lin, Z. All-Inorganic Perovskite Nanocrystals with a Stellar Set of Stabilities and Their Use in White Light-Emitting Diodes. ACS Appl. Mater. Interfaces 2018, 10 (43), 37267–37276.
- (50) Lu, H.; Tang, Y.; Rao, L.; Li, Z.; Ding, X.; Song, C.; Yu, B. Investigating the Transformation of CsPbBr₃ Nanocrystals into Highly Stable CsPbBr₃/Cs₄PbBr₆ Nanocrystals Using Ethyl Acetate in a Microchannel Reactor. *Nanotechnology* **2019**, *30* (29), 295603.
- (51) Ralaiarisoa, M.; Busby, Y.; Frisch, J.; Salzmann, I.; Pireaux, J. J.; Koch, N. Correlation of Annealing Time with Crystal Structure, Composition, and Electronic Properties of CH₃NH₃PbI_{3-x}Cl_x Mixed-Halide Perovskite Films. *Phys. Chem. Chem. Phys.* **2017**, *19* (1), 828–836.
- (52) Liu, M.; Zhong, G.; Yin, Y.; Miao, J.; Li, K.; Wang, C.; Xu, X.; Shen, C.; Meng, H. Aluminum-Doped Cesium Lead Bromide Perovskite Nanocrystals with Stable Blue Photoluminescence Used for Display Backlight. *Adv. Sci. (Weinh)* **2017**, *4* (11), 1700335.
- (53) Liu, Y.; Pan, G.; Wang, R.; Shao, H.; Wang, H.; Xu, W.; Cui, H.; Song, H. Considerably Enhanced Exciton Emission of CsPbCl₃ Perovskite Quantum Dots by the Introduction of Potassium and Lanthanide Ions. *Nanoscale* **2018**, *10* (29), 14067–14072.
- (54) Pazhanivelu, V.; Selvadurai, A. P. B.; Zhao, Y.; Thiyagarajan, R.; Murugaraj, R. Room Temperature Ferromagnetism in Mn Doped ZnO: Co Nanoparticles by Co-Precipitation Method. *Phys. B* **2016**, 481, 91–96.
- (55) Othman, A. A.; Osman, M. A.; Ibrahim, E. M. M.; Ali, M. A.; Abd-Elrahim, A. G. Mn-Doped ZnO Nanocrystals Synthesized by Sonochemical Method: Structural, Photoluminescence, and Magnetic Properties. *Mater. Sci. Eng., B* **2017**, *219*, 1–9.
- (56) Xu, S.; Xu, X.; Wang, C.; Zhao, Z.; Wang, Z.; Cui, Y. Theoretical and Experimental Investigation of Doping M in ZnSe (M

- = Cd, Mn, Ag, Cu) Clusters: Optical and Bonding Characteristics. Luminescence 2016, 31 (2), 312–316.
- (57) Parobek, D.; Roman, B. J.; Dong, Y.; Jin, H.; Lee, E.; Sheldon, M.; Son, D. H. Exciton-to-Dopant Energy Transfer in Mn-Doped Cesium Lead Halide Perovskite Nanocrystals. *Nano Lett.* **2016**, *16* (12), 7376–7380.